Springer

Acta Mechanica Sinica

CrossMark click for updates

• RESEARCH PAPER •

Acta Mech. Sin., Vol. 40, 324012 (2024)
https://doi.org/10.1007/s10409-024-24012-x

Reflection behavior of insensitive explosive detonation propagating around a cylinder

Zixuan Zhang[1,2], Yuan Wang[1], Xiaomian Hu[1], and Haitao Chen[1*]

[1] *Institute of Applied Physics and Computational Mathematics, Beijing 100094, China;*
[2] *Graduate School of China Academy of Engineering Physics, Beijing 100088, China*

Received January 9, 2024; accepted February 23, 2024; published online June 12, 2024

Insensitive explosive detonation has wide applications in compressing and driving inert materials, and thereby the interaction between detonation and inert materials has received more attention. In this paper, a two-dimensional numerical simulation based on the Euler multiphase flow framework is used to investigate the reflection behavior of the insensitive explosive detonation propagating around a cylinder. The results show that there is a critical incident angle, defined as transition angle for detonation propagating around the cylinder, below which the regular reflection (RR) on the cylinder surface is observed. When the incident angle is greater than the transition angle, RR changes to Mach reflection. This transition angle is larger than that obtained by polar curve theory and the change of incident angle is used to interpret above phenomenon. In addition, the influence of cylindrical radius and detonation reaction zone width on the reflection behavior is examined. As the cylindrical radius increases, the height of Mach stem increases while the transition angle decreases and gradually approaches the value in pole curve theory. Von Neumann reflection is observed when the reaction zone width is relatively small. This is because the energy release rate in the reaction zone is high for small reaction zone width, resulting in the formation of a series of compression waves near the cylindrical interface.

Insensitive explosive detonation, Cylindrical inert material, Reflection behavior

Citation: Z. Zhang, Y. Wang, X. Hu, and H. Chen, Reflection behavior of insensitive explosive detonation propagating around a cylinder, Acta Mech. Sin. 40, 324012 (2024), https://doi.org/10.1007/s10409-024-24012-x

1. Introduction

The detonation wave consists of a chemical reaction zone and leading shock. The leading shock compresses the unreacted mixture to a high pressure and density. The compressed mixture reacts dramatically and release energy to sustain the propagation of leading shock. The detonation speed of insensitive explosives is 6-8 mm/μs and the pressure at Von Neumann state is above 30 GPa, which can be used to compress and drive the confinement materials. The interaction between the detonation wave and the confinement materials can affect the compression and driving properties. Therefore, a large number of references have studied the interaction between detonation waves and confinement materials [1-3].

Short and Quirk [2], and Aslam and Bdzil [3] investigated the influence of confinement materials on the detonation wavefront curve, and found that the confinement materials with low impedance have a great effect on the curvature of the detonation waves and cause the wavefront curve obviously. The study by Short et al. [4] found that the influence of the thickness of the confining medium on the propagation process of the detonation wave is related to the acoustic impedance of the confining medium. When the acoustic impedance of the confining medium is small, the angular velocity of detonation propagation first increases and then remains unchanged with the thickness of the confining medium. When the acoustic impedance of the confining medium is large, the angular velocity of detonation wave propagation first increases, then decreases with the thickness of the confining medium, and finally remains unchanged. The study investigated by Ioannou and Nikiforakis [5] dis-

*Corresponding author. E-mail address: chen_haitao@iapcm.ac.cn (Haitao Chen)
Executive Editor: Ming Dong

© The Chinese Society of Theoretical and Applied Mechanics and Springer-Verlag GmbH Germany, part of Springer Nature 2024

cussed the desensitization and secondary initiation of insensitive explosives when diffracted on inert materials. Short et al. [6] studied the influence of low density interlayer between condensed matter explosive and finite thickness dense metal confined material on stable detonation propagation through two-dimensional (2D) numerical simulation. The results show that: For thinner interlayers, a shock-driven subsonic flow develops in the interlayer, transferring the disturbance from the metal layer to the explosive layer, and the detonation velocity decreases as the width of the interlayer increases. For wider interlayers, there will be a Mach stem structure in the interlayer, causing a reflected shock wave in the explosive. Anderson et al. [7] studied the effect of 1,3,5,7-Tetranitro-1,3,5,7-tetrazocane (HMX) content on the wavefront and detonation velocity of explosives confined by inert materials.

The above studies involve the material properties of the confining medium. The interaction between detonation waves and confining medium is also influenced by the geometric configuration feature of the confining medium. The study by Ben-Dor [8] found that the reflection behavior of shock waves on the surface of the confining medium is related to the incident angle. As the incidence angle increases, the reflection is regular reflection (RR), Mach reflection (MR), or von Neumann reflection (vNR). However, studies on the reflection behavior at the interface mainly focus on gas-phase detonation [9-11], while there are few studies on condensed-phase detonation waves. Li and Ning [12] investigated the reflection behavior of gas-phase detonation waves at convex interfaces. They found that compared with the reflection of the detonation wave on the wedge surface, the reflection behavior on the convex surface has hysteresis, that is, the transition angle from RR to MR is larger for convex surface reflection. Bdzil et al. [13,14] studied the reflection behavior of detonation waves from insensitive explosives on a rigid wedge surface and evaluated the influence of reaction rate models on the reflection behavior. When the reaction rate model is considered, the pressure gradient behind the detonation front is more obvious, and the vNR can be observed at a large incident angle.

Based on the above considerations, a 2D numerical simulation program based on the Euler multiphase flow framework is used to study the reflection behavior of the detonation wave of insensitive explosives propagating around a cylinder, and evaluate the influence of the cylinder radius and the detonation reaction zone width, Δ_r, on the reflection behavior of detonation propagating around the cylinder.

2. Numerical models and methods

2.1 Numerical model

This paper considers 2D detonation propagation around a cylinder. The numerical model is depicted in Fig. 1. The computational domain consists of insensitive explosive PBX9502 and cylindrical inert material iron (Fe). To initiate the detonation of insensitive explosive PBX9502, high pressure is used on the left side of the computational domain. The reaction zone width of the detonation wave is w. As the detonation propagates to the right side, it passes the cylindrical surface with a radius of r and the reflection phenomenon on the cylindrical surface can be observed. The free boundary condition is used on the left and right sides and solid wall boundary conditions is adopted for the top and bottom sides.

2.2 Numerical method

2.2.1 *Governing equation*

The 2D code based on the Euler multiphase flow framework is used for detonation propagation around the cylinder [15]. The continuity equation, momentum equation and energy equation are:

$$\frac{\partial}{\partial t}\begin{bmatrix}\rho\\ \rho u_1\\ \rho u_2\\ E\end{bmatrix}+\frac{\partial}{\partial x_1}\begin{bmatrix}\rho u_1\\ \rho u_1^2+p\\ \rho u_1 u_2\\ \rho u_1(E+p)\end{bmatrix}+\frac{\partial}{\partial x_2}\begin{bmatrix}\rho u_2\\ \rho u_1 u_2\\ \rho u_2^2+p\\ \rho u_2(E+p)\end{bmatrix}=\mathbf{0}, \tag{1}$$

ρ, u_1, u_2, p, and E represent density, x-direction velocity, y-direction velocity, pressure, and total energy, respectively.

2.2.2 *Reaction rate model*

The reaction rate model used in the present simulation is:

$$R = A(1-\lambda)^v p^n, \tag{2}$$

A, v, and n are constants of the reaction rate model. In the current calculation, v and n are fixed at $v = 0.5$ and $n = 1$, which is the same as that in Ref. [15]. In order to study the effect of reaction zone width on the propagation process of detonation waves around a cylinder, A changes from 1 to 20 and the corresponding variation of reaction process variables λ with A is shown in Fig. 2. As A increases, the width of the reaction zone (Δ_r) decreases. The reaction zone width is the length from $\lambda = 0$ to $\lambda = 0.99$.

2.2.3 *Equation of state (EOS)*

The Mie-Gruneisen EOS is considered in the present nu-

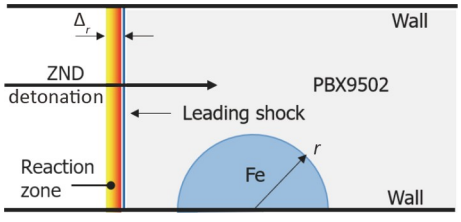

Figure 1 Schematic of detonation propagation around a cylinder.

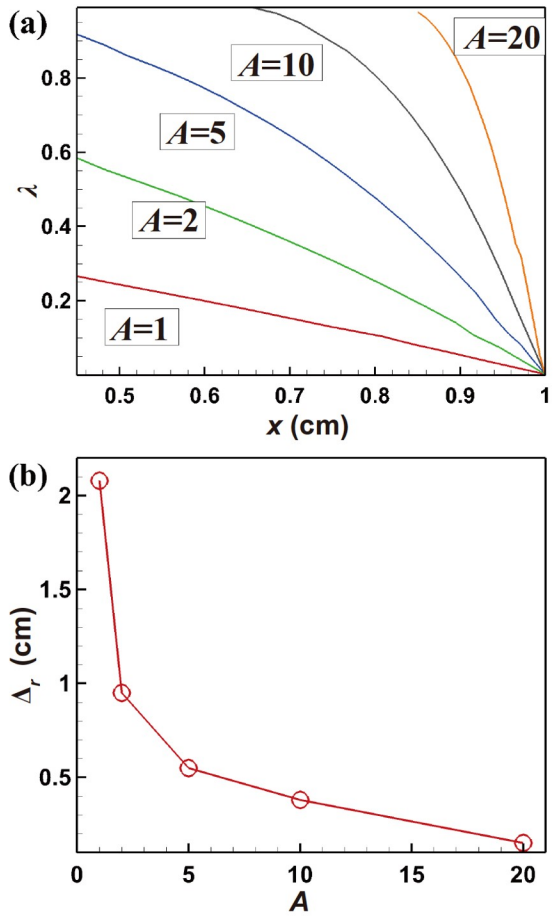

Figure 2 (a) Spatial distribution of reaction process variables λ for different A; (b) variation of reaction zone width with A.

merical simulation [2]:

$$p(\rho, e) = p_{\text{ref}} + \Gamma(\rho)\rho[e - e_{\text{ref}}(\rho)], \tag{3}$$

p_{ref} and e_{ref} are the reference pressure and reference specific internal energy, respectively:

$$p_{\text{ref}} = \frac{\rho_0 c^2 f}{(1-sf)^2}, \quad e_{\text{ref}} = \frac{c^2 f^2}{2(1-sf)^2}, \tag{4}$$

$U_s = c + su_p$, c is the sound speed at ambient pressure, U_s is the shock speed, u_p is the particle speed, and s is the slope, f is the change in relative density.

$$f = 1 - \frac{\rho_0}{\rho}, \tag{5}$$

the subscript 0 represents the initial confiner state and Γ is the Gruneisen gamma material parameter. Parameters for inert materials Mie-Gruneisen EOS are cited from Ref. [3] and listed in Table 1.

Jones-Wilkins-Lee (JWL) EOS for unreacted explosives and reacted products are used [16]:

$$p = Ae^{-R_1 v} + Be^{-R_2 v} + \frac{\omega C_V T}{V}, \tag{6}$$

where V is relative volume, T is temperature, ω is the Gruneisen coefficient, C_V is the average heat capacity, A, B, R_1, R_2 are constants. Parameters for PBX9502 are taken from Ref. [4] and listed in Table 2.

Table 1 Parameter for Mie-Gruneisen EOS

Parameter	ρ_0 (g/cm^3)	c (cm/μs)	s	Γ
Fe	7.85	0.3955	1.58	2.01

2.2.4 *Mixed rules*

The mass fraction of reactants and products in the mixture is determined by ϕ_r, and the mass fraction of inert materials is determined by $\phi_i = 1 - \phi_r$, assuming no mass transform between the reactant and product [15]:

$$\frac{\partial \phi_r}{\partial t} + u_1 \frac{\partial \phi_r}{\partial x_1} + u_2 \frac{\partial \phi_r}{\partial x_2} = 0, \tag{7}$$

$$\frac{\partial \phi_i}{\partial t} + u_1 \frac{\partial \phi_i}{\partial x_1} + u_2 \frac{\partial \phi_i}{\partial x_2} = 0, \tag{8}$$

λ is the reaction process variable, $\lambda = 0$ represents the solid reactant, and $\lambda = 1$ represents the gaseous reaction product:

$$\frac{\partial \lambda}{\partial t} + u_1 \frac{\partial \lambda}{\partial x_1} + u_2 \frac{\partial \lambda}{\partial x_2} = R. \tag{9}$$

The specific volume $v = 1/\rho$ for the mixture is related to the volume v_k, $k = i$, s, and g (i: inert materials; s: solid reactant; g: gaseous product), the constituents by the weighted average

$$v = \phi_r[\lambda v_g + (1-\lambda)v_s] + (1-\phi_r)v_i. \tag{10}$$

Similarly, the internal energy for the mixture is related to those of the constituents by

$$e = \phi_r[\lambda e_g + (1-\lambda)e_s] + (1-\phi_r)e_i. \tag{11}$$

We assume pressure and temperature equilibrium:

$$p = p_i = p_s = p_g, \quad T_i = T_s = T_g. \tag{12}$$

The total energy for the mixture is given by

$$E = \rho e + \frac{1}{2}\rho\left(u_1^2 + u_2^2\right). \tag{13}$$

Substituting Eqs. (7) and (8) into Eq. (1), we get

$$\frac{\partial \mathbf{u}}{\partial t} + u_1 \frac{\partial \mathbf{f_1(u)}}{\partial x_1} + u_2 \frac{\partial \mathbf{f_2(u)}}{\partial x_2} = \mathbf{R}. \tag{14}$$

For this equation there are

Table 2 Parameters for PBX9502

Parameters	ρ_0 (g/cm^3)	A (100 GPa)	B (100 GPa)	R_1	R_2	ω	C_V (GPa/K)
Unreacted explosives	1.895	632.07	−0.04472	11.3	1.13	0.8938	2.487×10^{-5}
Reacted products	1.895	13.6177	0.7199	6.2	2.2	0.5	1×10^{-5}

$$\mathbf{u}=\begin{bmatrix}\rho\\ \rho u_1\\ \rho u_2\\ E\\ \rho\phi_r\\ \rho\lambda\end{bmatrix},\quad \mathbf{f_1(u)}=\begin{bmatrix}\rho u_1\\ \rho u_1^2+p\\ \rho u_1u_2\\ \rho u_1(E+p)\\ \rho u_1\phi_r\\ \rho u_1\lambda\end{bmatrix},$$
$$\mathbf{f_2(u)}=\begin{bmatrix}\rho u_2\\ \rho u_1u_2\\ \rho u_2^2+p\\ \rho u_2(E+p)\\ \rho u_2\phi_r\\ \rho u_2\lambda\end{bmatrix},\quad \mathbf{R}=\begin{bmatrix}0\\0\\0\\0\\0\\ \rho R\end{bmatrix}. \tag{15}$$

2.3 Numerical verification

The reaction zone width for PBX9502 is around 2 mm, the grid size used in the numerical simulation is 0.02 mm and there are 100 grids within a reaction zone width. In order to verify the effectiveness of numerical calculations, we conducted a simulation for detonation propagation of arc shaped explosives in the surrounding confining medium as shown in Fig. 3(a) and (b). The results indicate that the steady-state detonation wave propagates along an arc at a constant angular velocity of 0.1146 rad/μs, which is close to the experimental result of 0.1106 rad/μs [4]. In addition, the wavefront curve obtained by numerical simulation is consistent with the experimental and simulation results [4]. Therefore, the numerical simulation program and method used in the present work are effective. Besides, the cylindrical radius considered in the present work is in the range of 3.0 mm to 15.0 mm, which is two orders larger than the mesh size of 0.02 mm at least. Therefore the cylindrical surface or the interface between the detonation wave and cylindrical surface can be greatly resolved.

3. Results and discussion

When detonation propagates around a cylinder, reflection behavior occurs on the cylindrical surface. We assess the effects of the incident angle, cylindrical radius, and reaction zone width on the reflection behavior.

3.1 Reflection behavior of detonation waves around cylindrical surfaces

Depending on the incident angle, detonation reflection on the cylindrical surface may be RR, MR, and vNR. In this subsection, we evaluate the effect of incident angle on the reflection behavior for a fixed cylindrical radius of r = 0.5 cm and parameter A = 10.

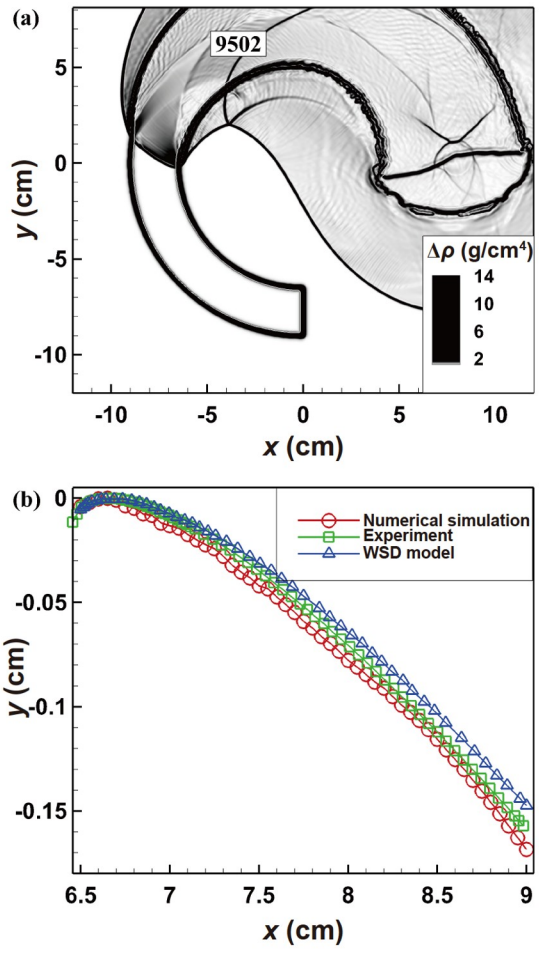

Figure 3 (a) Density gradient contour for steady-state detonation sweeping an arc. (b) Detonation wavefront loci in experiment [4], WSD model data (grid size 0.025 mm) [4], and numerical simulation.

Figure 4 shows the reflection behavior of a detonation wave propagating around a cylinder for θ = 40°. The RR is observed at the cylindrical surface. There exists a triple point at the cylindrical surface, which consists of an incident detonation wave, a reflected shock wave, and a transmitted shock wave. Due to the relatively high acoustic impedance of the inert material Fe (see Table 1), the transmitted shock wave surface lags behind the incident shock wave surface. The pressure and density increase behind the reflected shock wave.

As the detonation wave propagates forward, the incident angle increases. Figure 5 shows the detonation propagating around a cylinder for θ = 65°. The MR is observed at the cylindrical surface. This indicates that there is a critical incident angle (i.e., transition angle θ_c), above which the RR transforms into MR. At this point, a certain height of Mach stem is formed on the surface of the cylinder, and the three wave point structure detaches from the cylinder surface, consisting of incident detonation wave, reflected shock wave, and Mach stem. The density and pressure behind the

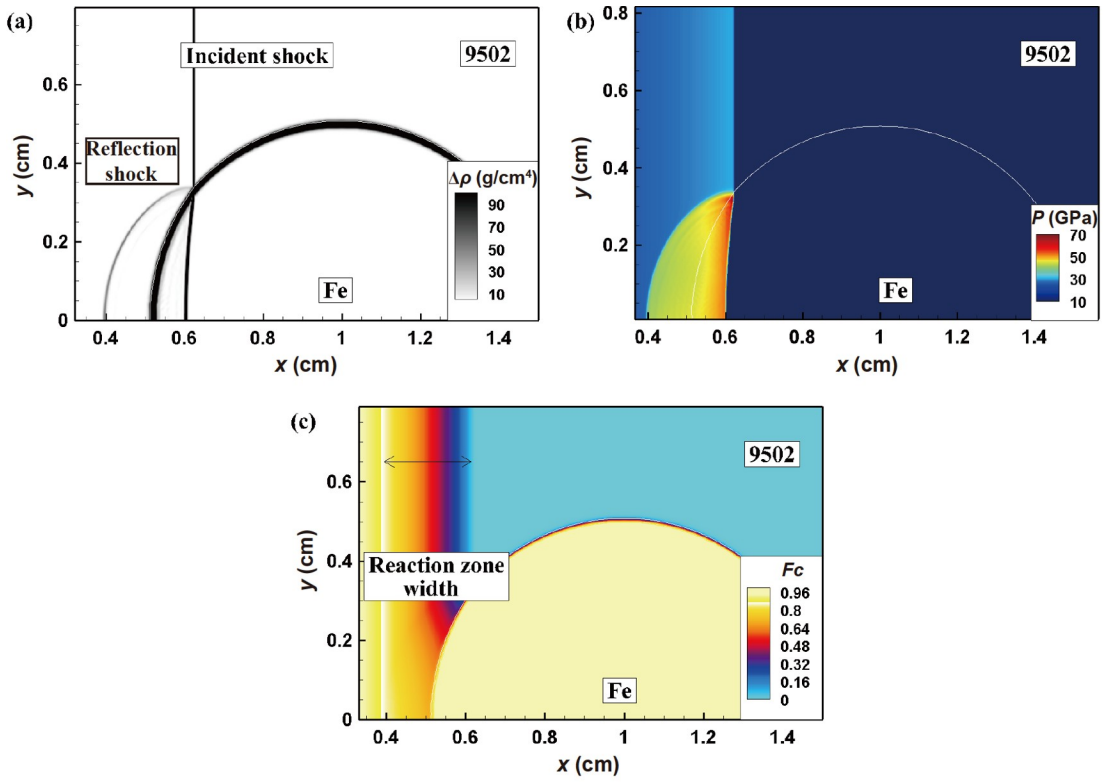

Figure 4 The contours of (a) density gradient, (b) pressure, and (c) mass fraction for detonation propagating around a cylinder with an incident angle of $\theta = 40°$.

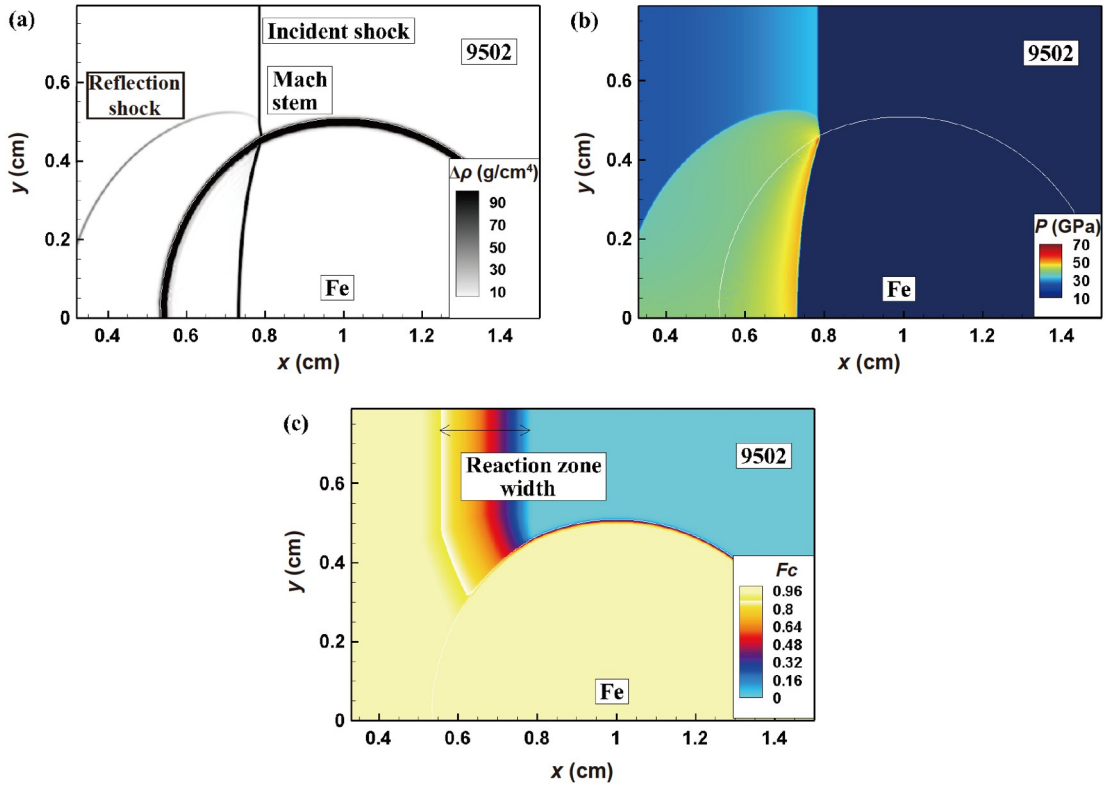

Figure 5 The contours of (a) density gradient, (b) pressure, and (c) mass fraction for detonation propagating around a cylinder with an incident angle of $\theta = 65°$.

Mach stem further increase.

As the detonation further propagates to the right side, the incident angle increases and the Mach stem height increases. When the incident angle θ = 88°, the height of the Mach stem is 0.18 cm (see Fig. 6), which is six times larger than 0.03 cm for θ = 65°. When the incident angle is greater than 90°, the propagation process of detonation waves around the cylinder undergoes diffraction behavior on the surface of the cylinder. In addition, Fig. 6 shows that when the incident angle approaches 90°, the flow field moving along the slipstream generates a jet at the interface, and the Mach stem is compressed and bent by the jet [17].

Figure 7 shows change of Mach stem height with incident angle. It is seen that the transition angle from RR to MR is about θ_c = 63°. In addition, as the incident angle increases, the height of the Mach stem increases linearly.

We use polar curve theory to study the reflection behavior of detonation propagating around a cylinder, and evaluate the influence of the cylindrical interface with different incident angles on the transition angle. Figure 8 shows the polar curve of reflected and transmitted shock waves at an incident angle of θ = 40°. The result shows that there is an

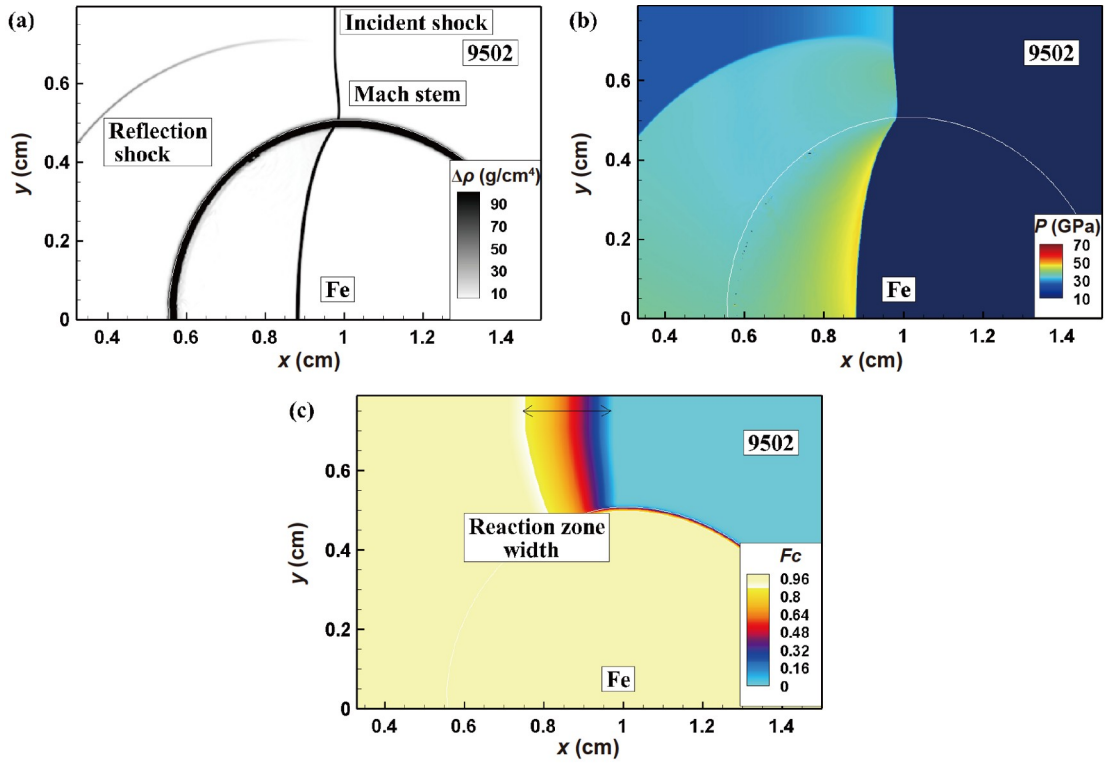

Figure 6 The contours of (a) density gradient, (b) pressure, and (c) mass fraction for detonation propagating around a cylinder with an incident angle of θ = 88°.

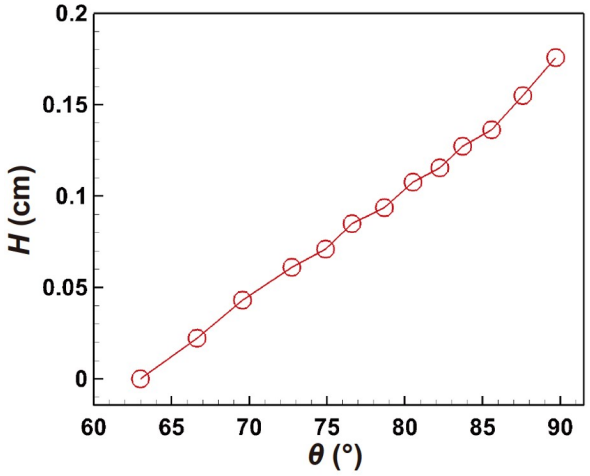

Figure 7 Change of Mach stem height with incident angle.

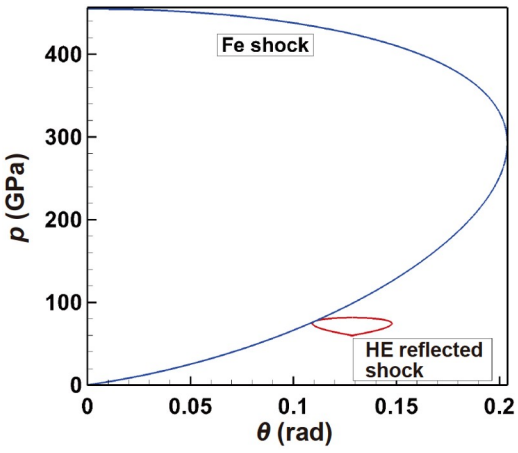

Figure 8 Polar curve distribution of reflection shock and transmitted shock of inert materials at an incident angle θ = 40°.

intersection point between the polar curves of the reflected shock wave and the transmitted shock wave for $\theta = 40°$. The Mach stem forms, and the RR changes to MR. Comparing the polar curve theory with the numerical calculation, the transition angle in the numerical calculation is $\theta_c = 63°$, which is much larger than the results obtained from the polar curve theory. Similar conclusions were also obtained in reference [18]. The reason is that the transition angle obtained by polar curve theory is under quasi-steady reflection. While the present work considers the detonation propagating around the cylinder with a variable incident angle and thus the reflection is non quasi-steady. Fluid on the cylinder surface needs to meet the non-penetrating condition. Figure 9 shows the change of reflected wave direction relative to the incident wave as the detonation propagating across the cylindrical surface. It is seen that the reflected shock wave undergoes relative motion in the direction of the incident wave, resulting in the increase in the Mach number of the flow field behind the wave, detonation propagating around the cylinder needs to satisfy the sound velocity criterion of MR only at a larger incident angle [19].

3.2 The influence of cylindrical radius

In this subsection, we consider the reflection behavior for detonation propagating around a cylinder at a fixed incident angle of $\theta = 82°$ and a fixed value of $A = 10$. The influence of the cylinder radius on the reflection behavior is assessed.

Figure 10 shows the detonation reflection behavior for different cylindrical radii and fixed incident angle of $\theta = 82°$. Similar detonation reflection processes are observed for different cylindrical radii. However, changing the cylindrical radius can significantly affect the height and transition angle of the Mach stem.

Figure 11(a) shows the change of Mach stem height with incident angle under different cylindrical radii. When the radius of the cylinder is the same, the height of the Mach stem increases with the incident angle. Increasing the cylindrical radius can significantly increase the height of the Mach stem when the incident angle is fixed. For $\theta = 90°$, the Mach stem height is 0.24 cm at $r = 0.7$ cm, which is around three times larger than the Mach stem height of 0.086 cm at $r = 0.3$ cm. In Fig. 11(b), the Mach stem height is normal-

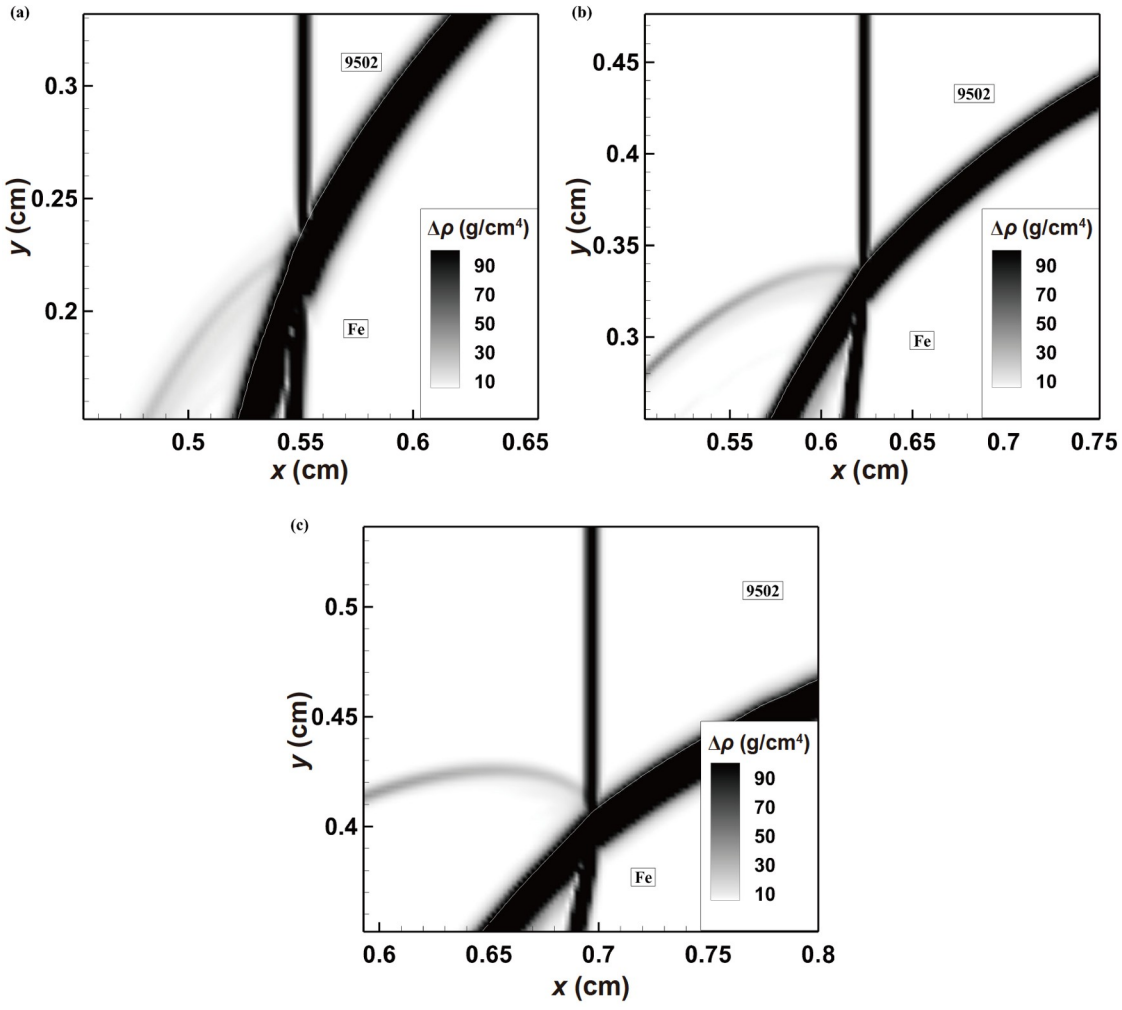

Figure 9 The change of reflected wave direction relative to incident wave at different time. (a) t =0.8 μs, (b) t =0.9 μs, (c) t =1.0 μs.

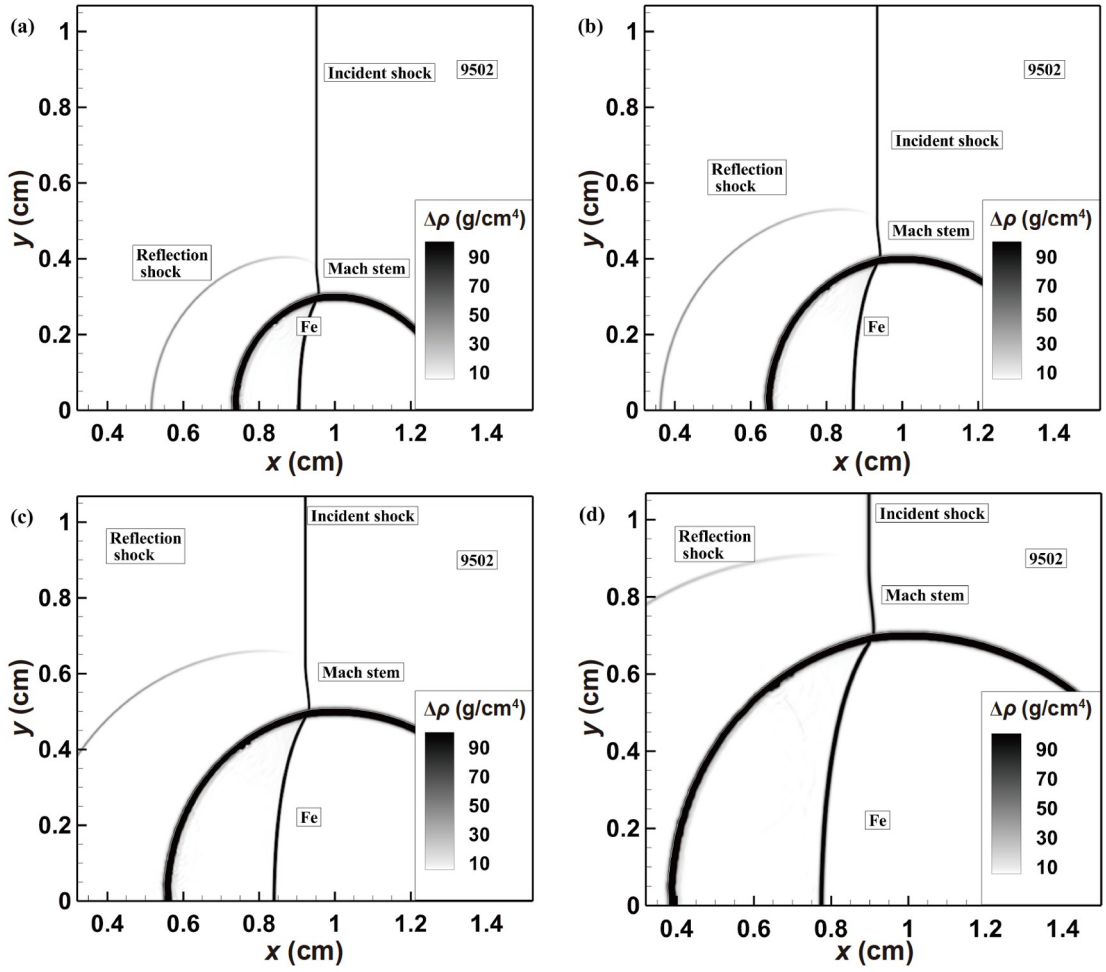

Figure 10 Density gradient contours for detonation propagating around a cylinder with different values of cylindrical radius. (a) r = 0.3 cm, (b) r = 0.4 cm, (c) r = 0.5 cm, and (d) r = 0.6 cm.

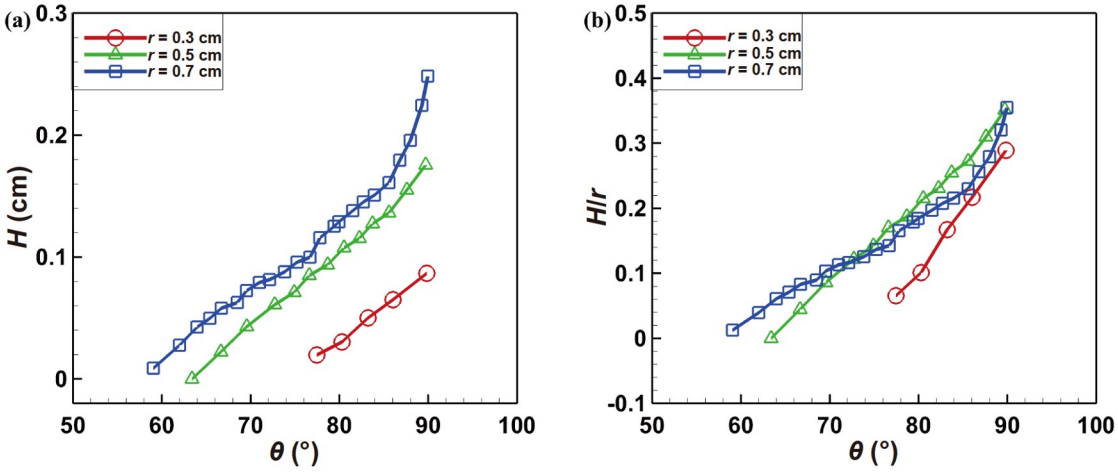

Figure 11 The variation of (a) Mach stem height (H) and (b) normalized Mach stem height by cylindrical radius (H/r) with incident angle at different cylindrical radii.

ized by cylindrical radius. For the same incident angle, the normalized Mach stem heights have a small difference for different cylindrical radii, which indicates that the Mach stem height has self-similarity. This is because the reaction zone does not change for different cylindrical radii.

Figure 12 shows the variation of the transition angle θ_c

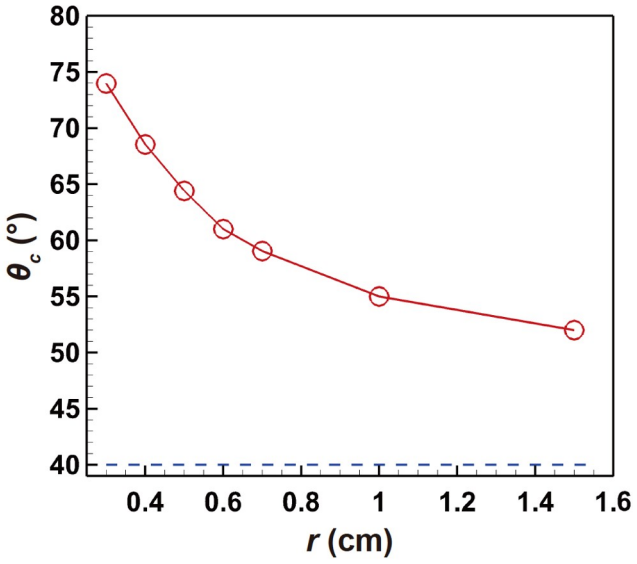

Figure 12 Change of transition angle (θ_c) with the cylindrical radius. The solid line represents the numerical calculation result, and the dashed line represents the theoretical result obtained by the polar curve theory.

with the cylindrical radius. The results indicate that the transition angle decreases with the cylindrical radius, and then approaches the value of $\theta_c = 40°$ obtained by the polar curve theory. This is because the smaller the radius, the faster the flow field after the reflected shock wave needs to be adjusted to adapt to the changing interface, resulting in a higher Mach number, thereby, the sound velocity criterion of MR needs to be satisfied at a larger incident angle.

3.3 The influence of reaction zone width

In this subsection, we consider the reflection behavior for detonation propagating around a cylinder for a fixed incident angle of $\theta = 80°$ and cylindrical radius of $r = 0.5$ cm but different reaction zone width and assess the effect of reaction zone width on the detonation reflection behavior.

Figure 13 shows the reflection behavior for detonation propagating around a cylinder with different A. We know that reaction zone width decreases with A (see Fig. 2). For $A = 0.5$ with a wide reaction zone, obvious reflected shock

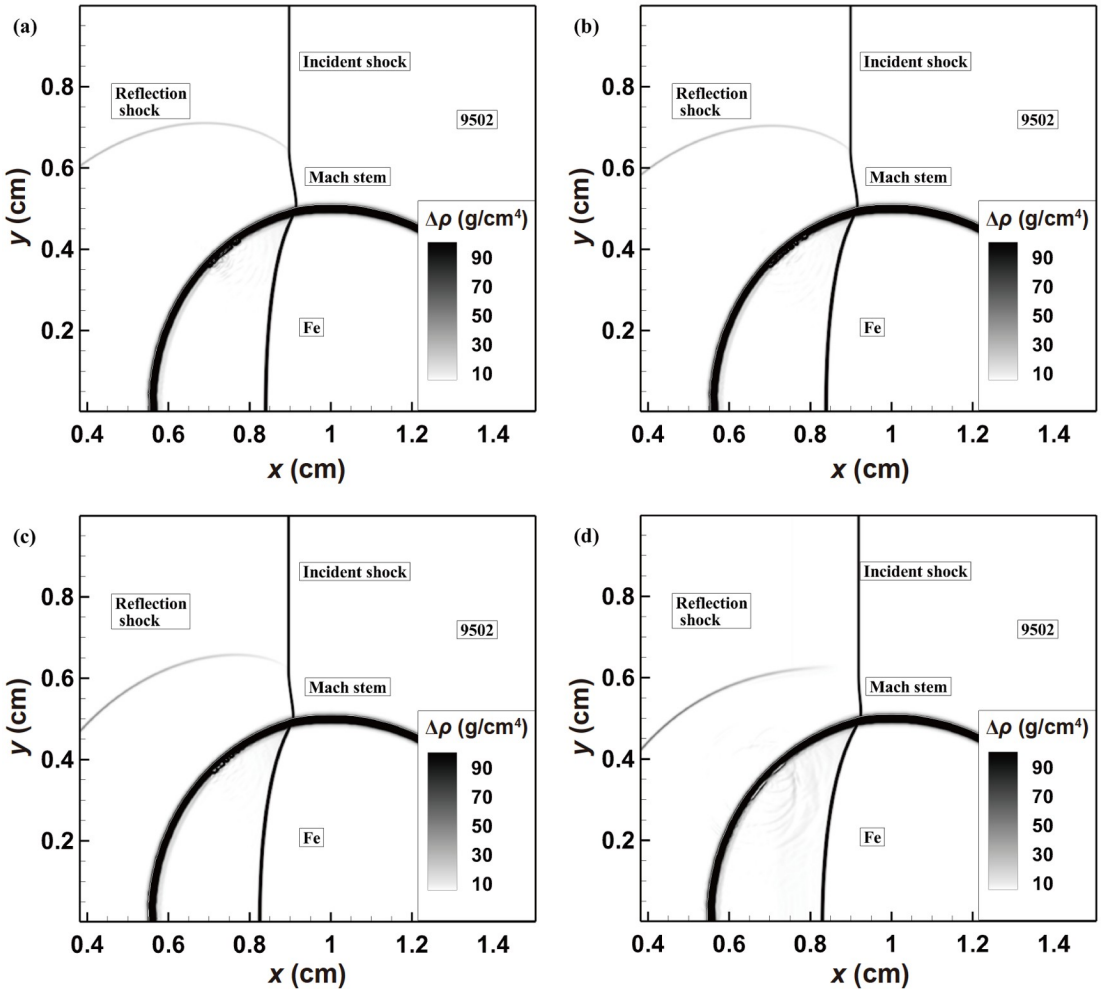

Figure 13 Density gradient contours for detonation propagating around a cylinder with fixed incident angle of $\theta = 80°$ and cylindrical radius of $r = 0.5$ cm but different reaction rate model parameters. (a) $A = 0.5$, (b) $A = 1$, (c) $A = 5$, and (d) $A = 20$.

waves and the triple point structure can be observed. As A increases (reaction zone width decreases), the triple point structure becomes blurred. For A = 20 (the reaction zone width is the smallest), it is difficult to observe the reflected shock wave and slip-stream near the reaction zone. Meanwhile, the detonation reflection on the cylindrical surface is a vNR. The vNR is a set of compressed waves of finite strength. The formation of vNR is due to the rapid energy release rate caused by the narrowing of the reaction zone width, which causes the disturbance propagation speed of the leading shock wave at the cylinder surface to exceed the speed of the Mach stem height increase [20], resulting in a series of compression waves near the cylinder surface. Therefore, the variation of reaction zone width results in different interactions between the detonation and inert materials.

4. Conclusions

2D numerical simulation based on the Euler multiphase flow framework is used to study the reflection behavior of the insensitive explosive detonation on the cylindrical surface. The effects of cylindrical radius and reaction zone width on the reflection behavior of detonation wave are evaluated, and the variation of transition angle and Mach stem height with incident angles, cylinder radius and reaction zone width are obtained. The main conclusions are:

(1) For fixed cylindrical radius and reaction zone width, there is a critical incident angle, defined as the transition angle θ_c. When the incident angle is larger than the transition angle, the reflection of the detonation wave on the cylindrical surface changes from RR to MR. This transition angle based on the present simulation is larger than the value obtained by polar curve theory considering quasi-steady detonation reflection on the wedge surface. This is because the flow field behind the reflected shock wave needs to satisfy the non-penetration condition when the detonation propagates around the cylinder. In order to satisfy the sound speed criterion of RR to MR, it needs to obtain a lower Mach number at a larger incident angle.

(2) For fixed incident angle and reaction zone width, as the cylindrical radius increases, the height of the Mach stem increases while the transition angle decreases gradually and approaches the value of polar curve theory.

(3) For fixed incident angle and cylinder radius, when the reaction zone width is reduced to a certain value, vNR is observed and there is no obvious slip-stream or reflected shock waves on the cylindrical surface. This is because when the reaction zone width is small, the energy release rate of the reaction zone is fast, and the disturbance propagation speed of the leading shock wave at the cylinder surface exceeds the speed of the Mach stem height increase, resulting in a series of compression waves formation near the cylinder surface.

It is noted that the perturbation propagation in the subsonic region of the reaction zone has not been studied and the vNR has not been analyzed quantitatively. Besides, in this paper, we considered the detonation propagating across a convex cylinder, some other geometries, such as the concave cylinder, need to be considered in future work.

Conflict of interest *On behalf of all authors, the corresponding author states that there is no conflict of interest.*

Author contributions ***Zixuan Zhang:*** *Formal analysis (lead), Methodology (lead), Software (lead), Writing – original draft (lead).* ***Yuan Wang:*** *Writing – review & editing (supporting), Formal analysis (equal).* ***Xiaomian Hu:*** *Formal analysis (supporting), Supervision (lead).* ***Haitao Chen:*** *Investigation (supporting), Conceptualization (lead), Supervision (equal), Validation (supporting), Writing – review & editing (supporting).*

1 J. B. Bdzil, and D. S. Stewart, The dynamics of detonation in explosive systems, Annu. Rev. Fluid Mech. **39**, 263 (2007).
2 M. Short, and J. J. Quirk, High explosive detonation-confiner interactions, Annu. Rev. Fluid Mech. **50**, 215 (2018).
3 T. D. Aslam, and J. B. Bdzil, in Numerical and theoretical investigations on detonation confinement sandwich tests: Proceedings of the Thirteenth International Detonation Symposium, Norfolk, 2006.
4 M. Short, C. Chiquete, J. B. Bdzil, and J. J. Quirk, Detonation diffraction in a circular arc geometry of the insensitive high explosive PBX 9502, Combust. Flame **196**, 129 (2018).
5 E. Ioannou, and N. Nikiforakis, Multiphysics modeling of the initiating capability of detonators. II. Booster initiation, J. Appl. Phys. **129**, 025903 (2021).
6 M. Short, C. Chiquete, and J. J. Quirk, The influence of multi-layer confinement on detonation propagation in condensed-phase explosives, Proc. Combust. Inst. **38**, 3595 (2021).
7 E. K. Anderson, C. Chiquete, S. I. Jackson, R. I. Chicas, and M. Short, The comparative effect of HMX content on the detonation performance characterization of PBX 9012 and PBX 9501 high explosives, Combust. Flame **230**, 111415 (2021).
8 G. Ben-Dor, Shock Wave Reflection Phenomena (Springer, Berlin, 2007).
9 J. Li, J. Pan, C. Jiang, Y. Zhu, Y. Zhang, and A. Oluwaleke OJO, Numerical investigation on cellular detonation reflection over wedges with rounded corner, Acta Astronaut. **181**, 503 (2021).
10 X. Yuan, J. Zhou, X. Mi, and H. D. Ng, Numerical study of cellular detonation wave reflection over a cylindrical concave wedge, Combust. Flame **202**, 179 (2019).
11 C. Shi, Y. You, X. Zheng, and C. Zhu, Analytical model for curved-shock Mach reflection, Phys. Fluids **35**, 031702 (2023).
12 J. Li, and J. Ning, Experimental and numerical studies on detonation reflections over cylindrical convex surfaces, Combust. Flame **198**, 130 (2018).
13 B. J. Bdzil, M. Short, and J. J. Quirk, in Oblique interaction of detonation with inert material confinement: The effect on the reaction zone: Proceedings of the 15th (International) Detonation Symposium, San Francisco, 2014.
14 J. B. Bdzil, and M. Short, Theory of Mach reflection of detonation at glancing incidence, J. Fluid Mech. **811**, 269 (2017).
15 J. W. Banks, W. D. Henshaw, D. W. Schwendeman, and A. K. Kapila, A study of detonation propagation and diffraction with compliant confinement, Combust. Theor. Model. **12**, 769 (2008).
16 L. Michael, and N. Nikiforakis, A hybrid formulation for the numerical simulation of condensed phase explosives, J. Comput. Phys. **316**, 193 (2016).
17 X. Shi, Y. Zhu, J. Yang, and X. Luo, Mach stem deformation in

pseudo-steady shock wave reflections, J. Fluid Mech. **861**, 407 (2019).
18 B. W. Skews, and H. Kleine, Shock wave interaction with convex circular cylindrical surfaces, J. Fluid Mech. **654**, 195 (2010).
19 M. Geva, O. Ram, and O. Sadot, The regular reflection→Mach reflection transition in unsteady flow over convex surfaces, J. Fluid Mech. **837**, 48 (2018).
20 A. Cohen, and B. Skews, Very weak shock wave reflection off curved surfaces, Exp. Fluids **61**, 174 (2020).

钝感炸药爆轰波绕圆柱体传播行为研究

张子瑄, 王元, 胡晓棉, 陈海涛

摘要 钝感炸药爆轰被广泛应用在压缩和驱动惰性材料领域, 爆轰与惰性材料间的相互作用受到越来越多的关注. 本文采用基于欧拉多相流框架的二维数值模拟程序, 研究钝感炸药爆轰波绕圆柱体传播过程的反射特性. 研究结果表明, 存在临界入射角, 当入射角小于临界入射角时, 爆轰波绕圆柱传播时在圆柱体表面发生规则反射; 当入射角大于临界入射角时, 圆柱体表面的规则反射变为马赫数反射, 该临界入射角被定义为反射过渡角. 极曲线理论获得的反射过渡角明显小于计算结果, 该现象可以通过爆轰波绕圆柱传播过程中入射角的变化解释. 此外, 本文评估了圆柱半径和爆轰波反应区宽度对反射特性的影响. 增大圆柱半径可以增大马赫杆高度, 减小反射过渡角. 随着圆柱半径的增大, 反射过渡角逐渐接近极曲线理论值. 当反应区宽度较小时, 圆柱表面形成冯诺依曼反射, 这是因为反应区宽度越小, 反应区能量释放率越高, 从而导致圆柱表面附近形成一系列压缩波.